Title
Investigating the Doping Mechanism of Pyrene Based Methacrylate Functional Conductive Binder in Silicon Anodes for Lithium-Ion Batteries

Journal
Journal of The Electrochemical Society, 164(4)

ISSN
0013-4651

Authors
Ling, Min
Liu, Michael
Zheng, Tianyue
et al.

Publication Date
2017

DOI
10.1149/2.0011704jes

Peer reviewed

Investigating the Doping Mechanism of Pyrene Based Methacrylate Functional Conductive Binder in Silicon Anodes for Lithium-Ion Batteries

Min Ling,[a] Michael Liu,[b] Tianyue Zheng,[a] Ting Zhang,[a] and Gao Liu[a,*,z]

[a]*Applied Energy Materials Group, Energy Storage and Distributed Resources Division, Lawrence Berkeley National Laboratory, Berkeley, California 94720, USA*
[b]*Materials Science and Engineering, University of California, Berkeley, Berkeley, California 94720, USA*

The doping mechanism of poly (1-pyrenemethyl methacrylate) (PPy) is investigated through electrochemical analytical and spectroscopic method. The performance of PPy as a Si materials binder is studied and compared with that of a commercial available lithium polyacrylate (PAALi) binder. The pyrene moiety consumes lithium ions according to the cyclic voltammogram (CV) measurement, as a doping to the PPy binder. Based on the lithium consumption, PPy based Si/graphite electrode doping is quantified at 1.1 electron/pyrene moiety. The PPy binder based electrodes surface are uniform and crack free during lithiation/delithiation, which is revealed through Scanning electron microscope (SEM) imaging.
 [DOI: 10.1149/2.0011704jes]

Manuscript submitted November 21, 2016; revised manuscript received December 29, 2016. Published January 21, 2017.

Silicon exhibits an order of magnitude higher than that of the conventionally used graphite, meanwhile, dramatic volume change (ca. 300%) accompanied by high level of side reaction during battery operation disrupts the electrode integrity, and hinders the application of Si in commercial batteries.[1] Carbon black conductive additive is included in the electrode to improve electronic conductivity. However, the conductive additive tends to be pushed away from the Si particles by volume expansion of Si, leading to broken electrical connections at the interface and capacity decay.[2,3] Traditionally, most research has been focused on modification of Si powders with improved properties, and less attention was devoted to electrode binder.[4–10] Functional electrode binders that aimed to enhance conductivity, combat severe volume changes and reduce side-reactions, have attracted significant attentions and intensive development efforts during the past decades.[11,12] Poly (1-pyrenemethyl methacrylate) (PPy),[13] is a unique functional conducting polymer materials, whose chemical and mechanical properties can easily controlled by facile radical based synthesis process. For PPy, the electric conductivity is originated from π-π stacking of pyrene side chains. When the pyrene moieties are connected to flexible backbones, they are close in position to be easily self-assembled into ordered structures,[14] to further enhance the electrical conductivity. To further clarify the conductive mechanism, we integrate the electrochemical response of the polymer in an electrochemical cell to verify the lithium ions doping into pyrene molecular. The lithiation to PPy is quantitatively measure through Circular Voltammetry (CV) measurements. The galvanostatic lithiation/delithiation properties of the graphite/Si electrode with lithium polyacrylate (PAALi) binder, and poly (1-pyrenemethyl methacrylate) (PPy) binder was also performed. The morphology transformation after lithiation/delithiation of the electrodes based on different binder is also recorded to reveal the mechanical property difference of the electrodes.[15]

Experimental

All reagents were purchased from Sigma-Aldrich or TCI America and used without further purification. MAGE, bought from Hitachi was used as the graphite anode. The nanoSi with a particle size of 50–70 nm is from Nanostructured and Amorphous Inc. PPy polymer is synthesized in our lab.[13] Celgard 2400 separator is obtained from Celgard. Lithium-ion electrolyte were purchased from BASF, including 1.0 M $LiPF_6$ in ethylene carbonate, diethyl carbonate (EC/DEC = 3/7 w/w) containing 30 wt% fluoroethylene carbonate (FEC).[30] 2325 coin cells were prepared using lithium metal as a counter electrode. The Linear sweep voltammograms were conducted between 0.005 V and 2 V at 0.02 mV/s using Biologic MPG-2 in coin cell configuration. The working electrode is the Si composite or polymer film on the Cu foil. The counter electrode is lithium foil. The electrolyte applied in CV tests is exactly the same as in the cycling cells. The Si mass loading for the electrodes as shown in Figures 1a, 1b, 1c and 1d is ca. 0.2 mg/cm^2.The polymer mass loading for the electrodes as shown in Figure 1e and 1f is ca. 0.02 mg/cm^2, corresponding to a thickness of ca. 120 nm. For the high loading composition, the PAALi based electrode is composed of 73 wt% MAGE, 15 wt% Si, 2 wt% Timical C45 and 10% PAALi. The PPy based electrode is composed of 73 wt% MAGE, 15 wt% Si and 12% PPy. Slurry was prepared through a low energy ball milling for 10 hours. SEM images of the composite electrode surface were collected with a JEOL JSM-7500F field emission scanning electron microscopy with an accelerating voltage of 15 kV using the high vacuum mode at room temperature.

Results and Discussion

To calculate the lithiation into PPy, we compare the performance of PAALi with PPy, as PAALi has the same polymer backbone as PPy materials.[16] This structure resemblance makes PAALi a good baseline material. To precisely calculate the lithium doping into the Si/graphite composite electrode, full lithiation is needed to guarantee the accuracy. Hence, the mass loading of Si is specially coated to be 0.2 mg/cm^2 to achieve full capacity. As the potential scans cathodically from the open circuit voltage of the Si anode at the first cycle, the solid electrolyte interface (SEI) starts to form between 0.5 V and 0.8 V due to the surface reaction with electrolyte.[17–25] Ideally, the SEI blocks further electrolyte side reaction and only the lithium ion can pass through the SEI film and lithiate into Si anode. This electrochemical lithiation process is reflected by the cathodic current as shown in Figure 1. As the potential is scanned back to 2.0 V, the lithium ions are delithiated from Si anode. According to the cyclic voltammograms (CV) profiles integration, the firstcycle coulombic efficiency (CE) for PAALi and PPy based Si anode is 69.5% and 55.3%, respectively. This implies that more lithium is consumed by PPy than PAALi in the first cycles. To quantify the amount of lithium ions that is consumed before lithiation into Si, the quantity of electric charge (Q) is integrated from the open circuit voltage (OCV) to 0.8 V as shown in Figure 1b and 1d. The equivalent specific capacity based on PAALi/Si electrode is calculated to be 256 mAh/g_{Si}, which is lower than that of the PPy/Si based electrode (279 mAh/g_{Si}). The additional lithiation capacity is the lithiation into the pyrene group. To exclude the interference of lithiation into Si, the polymers are coated directly onto the copper foil to form a thin film with a thickness

*Electrochemical Society Member.
[z]E-mail: gliu@lbl.gov

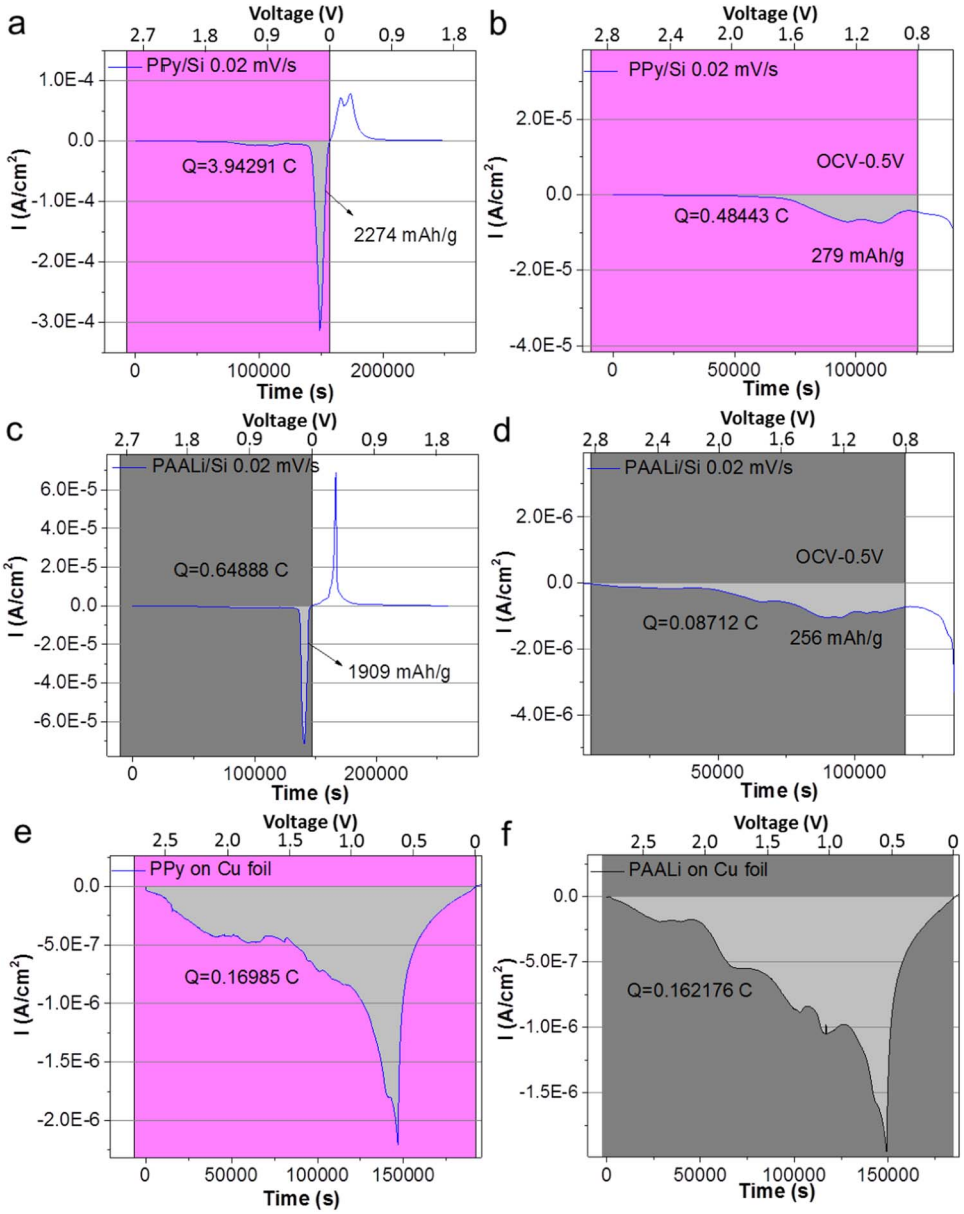

Figure 1. (a, b, c, d) Linear sweep voltammograms of the PPy/Si (1/2 wt%) and PAALi/Si (1/2 wt%) electrodes at 0.02 mV/s in 1.0 M $LiPF_6$ in ethylene carbonate, diethyl carbonate (EC/DEC = 3/7 w/w) containing 30 wt% fluoroethylene carbonate (FEC) electrolyte. (e, f) Linear sweep voltammograms of the PPy and PAALi film on Cu foil at 0.02 mV/s in ethylene carbonate, diethyl carbonate (EC/DEC = 3/7 w/w) containing 30 wt% fluoroethylene carbonate (FEC) electrolyte.

of around 1.0 micro-meter. The lithiation profiles are presented in Figures 1e and 1f. There is an apparent bump above 0.8 V which represents additional lithiation into pyrene group in PPy polymer. The percentage of the total additional lithiation is calculated to be 4.7% as integrated.[26]

To in-situ quantify the degree of lithium doping into the pyrene groups, PAALi and PPy are assembled into the graphite/Si composite electrodes for their identical backbones except the pyrene side chain groups in PPy. Targeting at a commercial energy density, the relatively high loading electrodes are assembled and cylced. The PPy and PAALi based electrode contains 3.06 and 3.10 mg/cm^2 Si/graphite composite respectively. The left Y axis in Figure 2a is plotted as mAh per gram of graphite/Si, which exhibits capacity twice as high as conventional graphite anode even after 100 cycles. Also, a significant areal capacity of more than 2.5 mAh/cm^2 is achieved and maintained stable for more than 200 cycles. Since the conductive PPy polymer could cover the surface of the silicon nanoparticles, the SEI film will form directly on the polymer surface. Due to the higher free volume of PPy polymer, the PPy based electrodes could reduce the continuous lithium consumption in SEI film, which result in a better capacity retention. The corresponding coulombic efficiency (CE) is shown in Figure 2b. The CE of the first cylce for PPy and PAALi is 82.8% and 89.1%, respectively. Assuming the extra irreversible lithium ions is consumed by pyrene group, the calculated electron into pyrene structure is 0.22 C. Consequently, the ratio of lithium ions to pyrene group is 1.1, which is calculated based on the mass of PPy polymer (0.59 mg) in the electrode.[27]

The effectiveness of functional PPy binder is further demonstrated by post analysis of the electrode. The cells are disassembled both in fully lithiated and delithiated states. The harvested electrodes are immersed in dimethyl carbonate (DMC) for 30 min and flushed three times prior to scanning electron microscope (SEM) images collection. When the PPy based electrode is in fully lithiated state, as shown in Figure 3g, Si particles (50–70 nm) expand to more than 100 nm uniformly after lithiation, indicating the high utilization of Si particles. In contrast, the expansion is less uniform for PAALi based electrodes

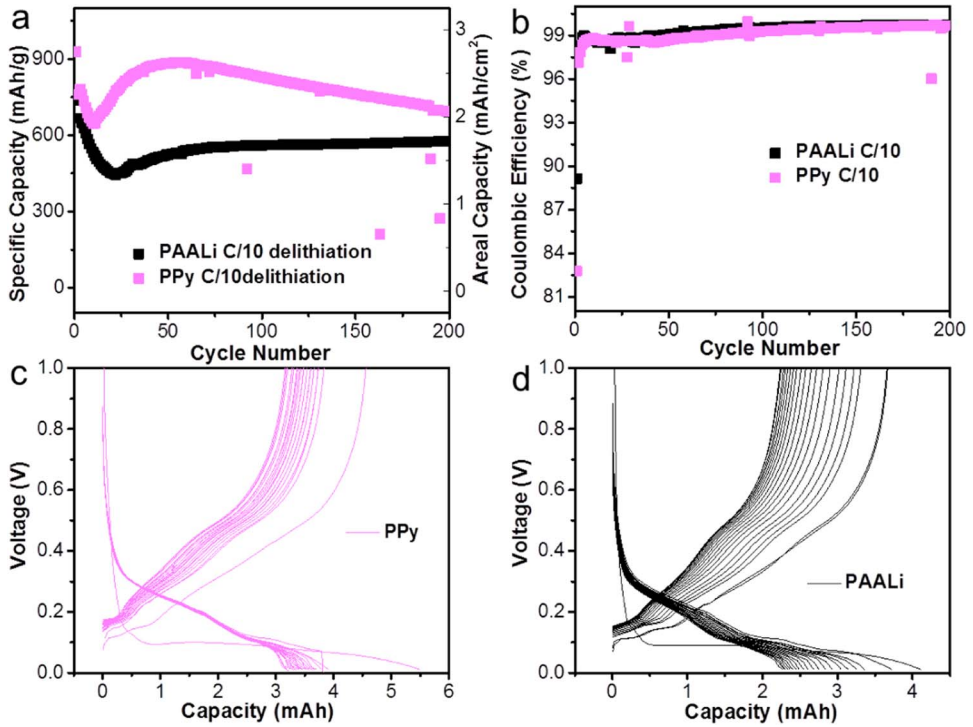

Figure 2. (a) Specific capacity (left Y axis) and areal capacity (right Y axis) vs. cycle number, (b) Coulombic efficiency vs. cycle number for electrodes based on PPy binder (PPy/Si/Graphite = 12/15/73 wt%) and PAALi binder. (PAALi/Carbon black/Si/Graphite = 10/2/15/73 wt%). The initial two cycles were at C/25, then C/10 for the long-term cycling. (c, d) Voltage profiles of PPy and PAALi based electrodes at the first 20 cycles, PPy shows much less capacity decay above 0.1 V, which implies the higher Si utilization for PPy based electrode.

(Figure 3e), which is also consistent with the cycle performances. This suggests that the PPy enhances the utilization of Si particles, critical to the success of Si/graphite composite anode. The mechanical uniformity of the PPy based electrode also improves, as cracks happen in PAALi based electrodes among the pristine, lithiated and delithiated electrodes, while there are no cracks in the PPy based electrodes in all cases as shown in Figure 3, indicating the better mechanical strength of PPy binder for the Si/graphite composite material.[7]

With the promising electrochemical performance illustrated above, the potential durability of PPy polymer binder is evaluated through Fourier Transform Infrared spectroscopy (FTIR) as shown in Figure 4. The signal is collected from the powders that harvest from the pristine and cycled electrodes. The disassembled electrodes are immersed in dimethyl carbonate (DMC) for 1 h and flushed cleaned three times. Indicated in the blue shadow highlighted wave numbers, it is clearly that the three main characteristic peaks of PPy are retained after 70

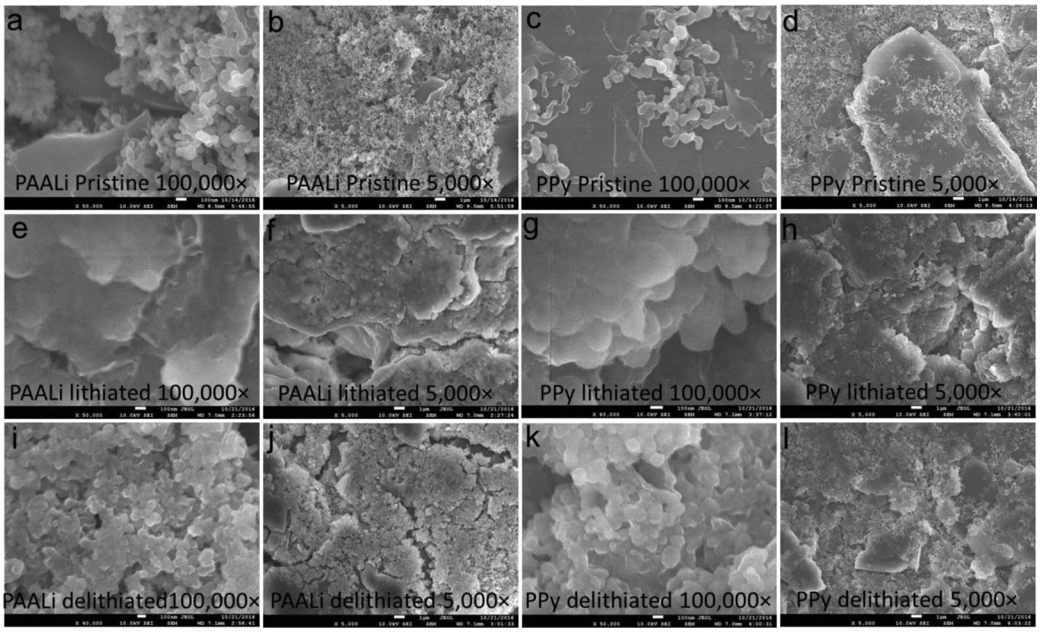

Figure 3. SEM images of PAALi and PPy based pristine, lithiated and delithiated Si/graphite electrodes with vary magnification.

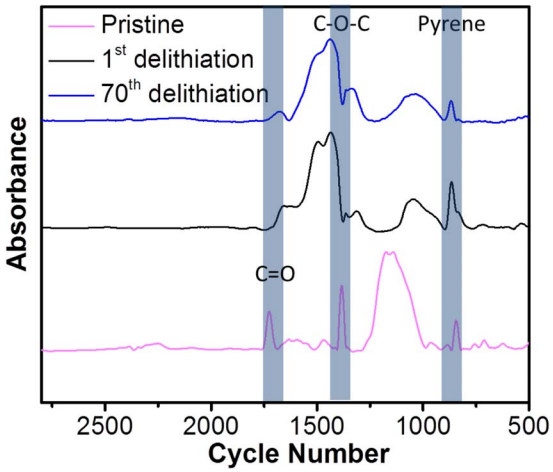

Figure 4. Fourier transform infrared (FTIR) spectra of the PPy based pristine and delithiated electrodes.

cycles lithiation/delithiation,[28] though the C-O-C vibration turns out to be broader due to the spectra overlapping from the electrolyte decomposition residues.[29] The spectroscopic analysis underlines the both the electrochemical and mechanic stability of PPy polymer in the Si based electrode.

Conclusions

Functional conductive polymer such as PPy can be a very effective conductive and adhesive agent for electrode fabrication. This study focuses on quantify the reactivity and stability of the functional polymer in very low potential, which is critical for the eventual application of the functional binders in the commercial battery. The higher utilization of Si for PPy based electrode has been proved through the voltage profiles and lithiated morphologies. The lithiation into PPy was revealed through the cyclic voltammograms (CV) integration. The degree of lithium doping was further quantified to be 1.1 Li^+/pyrene through the comparison of charge quantity between PAALi and PPy based electrode. The better mechanical strength of PPy to PAALi is demonstrated through SEM analyses. Finally, the stability of PPy is demonstrated by post analysis of the electrodes. Although this work is focus on the new PPy binders, these kinds of rigorous approaches of evaluation of the functional binders will provide useful information to compare the different binders develop by the community.

Acknowledgments

This work was funded by the Assistant Secretary for Energy Efficiency, Vehicle Technologies Office of the U.S. Department of Energy (U.S. DOE) under the Applied Battery Research (ABR) Programs. (ANL CAMP facilities for electrode and materials supplies) Synchrotron-based soft X-ray scattering and analysis is conducted at the Advanced Light Source (ALS), located at Lawrence Berkeley National Lab. All these projects and facilities are supported by the Director, Office of Science, Office of Basic Energy Sciences, of the U.S. Department of Energy, under Contract # DE-AC02-05 CH11231. The authors declare no competing financial interests.

References

1. S.-J. Park, H. Zhao, G. Ai, C. Wang, X. Song, N. Yuca, V. S. Battaglia, W. Yang, and G. Liu, *J. Am. Chem. Soc.*, **137**, 2565 (2015).
2. X. Su, Q. Wu, J. Li, X. Xiao, A. Lott, W. Lu, B. W. Sheldon, and J. Wu, *Advanced Energy Materials*, **4** (2014).
3. M. R. Zamfir, N. Hung Tran, E. Moyen, Y. H. Lee, and D. Pribat, *Journal of Materials Chemistry A*, **1**, 9566 (2013).
4. S. Xin, W. Qingliu, L. Juchuan, X. Xingcheng, A. Lott, L. Wenquan, B. W. Sheldon, and W. Ji, *Advanced Energy Materials*, **4**, 1300882 (23 pp.) (2014).
5. M. Ling, H. Zhao, X. Xiaoc, F. Shi, M. Wu, J. Qiu, S. Li, X. Song, G. Liu, and S. Zhang, *J. Mater. Chem. A*, **3**, 2036 (2014).
6. M. Ling, Y. Xu, H. Zhao, X. Gu, J. Qiu, S. Li, M. Wu, X. Song, C. Yan, G. Liu, and S. Zhang, *Nano Energy*, **12**, 178 (2015).
7. M. Ling, J. Qiu, S. Li, C. Yan, M. J. Kiefel, G. Liu, and S. Zhang, *Nano Lett.*, **15**, 4440 (2015).
8. M. T. McDowell, S. W. Lee, J. T. Harris, B. A. Korgel, C. Wang, W. D. Nix, and Y. Cui, *Nano Lett.*, **13**, 758 (2013).
9. N. Liu, Z. Lu, J. Zhao, M. T. McDowell, H.-W. Lee, W. Zhao, and Y. Cui, *Nat. Nanotechnol.*, **9**, 187 (2014).
10. M. Gu, X.-C. Xiao, G. Liu, S. Thevuthasan, D. R. Baer, J.-G. Zhang, J. Liu, N. D. Browning, and C.-M. Wang, *Scientific Reports*, **4** (2014).
11. I. Kovalenko, B. Zdyrko, A. Magasinski, B. Hertzberg, Z. Milicev, R. Burtovyy, I. Luzinov, and G. Yushin, *Science*, **334**, 75 (2011).
12. D. Munao, J. W. M. van Erven, M. Valvo, E. Garcia-Tamayo, and E. M. Kelder, *J. Power Sources*, **196**, 6695 (2011).
13. S.-J. Park, H. Zhao, G. Ai, C. Wang, X. Song, N. Yuca, V. S. Battaglia, W. Yang, and G. Liu, *J. Am. Chem. Soc.*, **137**, 2565 (2015).
14. Z. W. Seh, Q. Zhang, W. Li, G. Zheng, H. Yao, and Y. Cui, *Chemical Science*, **4**, 3673 (2013).
15. F. Luo, B. Liu, J. Zheng, G. Chu, K. Zhong, H. Li, X. Huang, and L. Chen, *J. Electrochem. Soc.*, **162**, A2509 (2015).
16. Z. J. Han, N. Yabuuchi, S. Hashimoto, T. Sasaki, and S. Komaba, *ECS Electrochemistry Letters*, **2**, A17 (2012).
17. U. S. Vogl, S. F. Lux, E. J. Crumlin, Z. Liu, L. Terborg, M. Winter, and R. Kostecki, *J. Electrochem. Soc.*, **162**, A603 (2015).
18. J.-H. Cho and S. T. Picraux, *Nano Lett.*, **14**, 3088 (2014).
19. T. Jaumann, J. Balach, M. Klose, S. Oswald, U. Langklotz, A. Michaelis, J. Eckerta, and L. Giebelera, *Phys. Chem. Chem. Phys.*, **17**, 24956 (2015).
20. X. Feng, J. Yang, X. Yu, J. Wang, and Y. Nuli, *J. Solid State Electrochem.*, **17**, 2461 (2013).
21. J. Bae, S.-H. Cha, and J. Park, *Macromol. Res.*, **21**, 826 (2013).
22. K. Bonjae, K. Hyunjung, C. Younghyun, L. Kyu Tae, C. Nam-Soon, and C. Jaephil, *Angewandte Chemie International Edition*, **51**, 8762 (2012).
23. L. B. Chen, X. H. Xie, J. Y. Xie, K. Wang, and J. Yang, *J. Appl. Electrochem.*, **36**, 1099 (2006).
24. J. H. Cho and S. T. Picraux, *Nano Lett.*, **14**, 3088 (2014).
25. M. Y. Nie, D. P. Abraham, Y. J. Chen, A. Bose, and B. L. Lucht, *J. Phys. Chem. C*, **117**, 13403 (2013).
26. C. de las Casas and W. Li, *J. Power Sources*, **208**, 74 (2012).
27. L. Yue, L. Zhang, and H. Zhong, *J. Power Sources*, **247**, 327 (2014).
28. M. J. Lacey, F. Jeschull, K. Edström, and D. Brandell, *J. Power Sources*, **264**, 8 (2014).
29. Z. W. Seh, Q. Zhang, W. Li, G. Zheng, H. Yao, and Y. Cui, *Chemical Science*, **4**, 3673 (2013).
30. W.-J. Zhang, *J. Power Sources*, **196**, 13 (2011).